# Techniques in the Moment Analysis of Net-proton Multiplicity Distributions in Heavy-Ion Collisions

Xiaofeng Luo,[1,2,*] Ji Xu,[1,2] Bedangadas Mohanty,[3] and Nu Xu[1,2,4]

[1] *Institute of Particle Physics, Central China Normal University, Wuhan, Hubei, 430079, China*
[2] *The Key Laboratory of Quark and Lepton Physics (Central China Normal University), Ministry of Education, Wuhan, Hubei, 430079, China*
[3] *National Institute of Science Education and Research, Bhubaneswar 751005, India*
[4] *Nuclear Science Division, Lawrence Berkeley National Laboratory, Berkeley, CA 94720, USA.*

(Dated: February 12, 2013)

Moments (Variance ($\sigma^2$), Skewness($S$), Kurtosis($\kappa$)) of multiplicity distributions of conserved quantities, such as net-baryon,net-charge and net-strangeness, are predicted to be sensitive to the correlation length of the system and connected to the thermodynamic susceptibilities computed in Lattice QCD and Hadron Resonance Gas (HRG) model. In this paper, we point out several measurement artifacts like centrality bin width effect, auto-correlation and centrality resolution effect in the moment analysis of net-proton multiplicity distributions in high energy heavy-ion collisions using the UrQMD model. We present methods to overcome these artifacts so that the extracted moments could be used to obtain physical conclusions. In addition we present methods to properly estimate the statistical errors in moment analysis.

PACS numbers: 25.75.Ld, 25.75.Dw



## I. INTRODUCTION

One of the main goals to perform heavy-ion collision experiments is to explore the phase structure of the QCD matter, such as search for the QCD critical point [1, 2] and the phase transition boundary between hadronic matter and partonic matter. Finite temperature Lattice QCD calculations predict that the transition from nuclear matter phase to Quark Gluon Plasma (QGP) phase is a smooth cross-over at high temperature and small $\mu_B$ [3], and a first order phase transition at large $\mu_B$ [4]. The corresponding transition temperature is about 170∼190 MeV [5]. Although many efforts have been made by theorist and experimentalist to locate the CP (Critical Point), its location or even existence is still not confirmed yet [6]. The first principle Lattice QCD calculation at finite $\mu_B$ is difficult to carry out due to the sign problem [1, 6]. Although many techniques, such as re-weighting, image baryon chemical potential and Taylor expansion, have been developed to overcome those problems and make the numerical QCD calculations at finite $\mu_B$ region, but with large uncertainties [7].

In heavy-ion collision, the moments (Variance ($\sigma^2$), Skewness($S$), Kurtosis($\kappa$)) of distributions of conserved quantities, such as net-baryon,net-charge and net-strangeness, are predicted to be sensitive to the correlation length [8] and to be connected to the thermodynamic susceptibilities computed in Lattice QCD [1, 9, 10] and in the Hadron Resonance Gas (HRG) [11] model. QCD based model calculation show that moments of particle multiplicity distributions are proportional to the higher power of the correlation length, such as third order cumulant $< (\delta N)^3 > \sim \xi^{4.5}$ and fourth order cumulant $< (\delta N)^4 > -3(\delta N)^2 > \sim \xi^7$ [8]. In statistics, skewness and kurtosis are widely used to characterize the properties of probability distributions. Skewness is used to describe the asymmetry property of distributions, while kurtosis describes their peakness. The higher moments of baryon number distributions are also directly connected to the corresponding baryon number susceptibilities in Lattice QCD and HRG model calculations [10, 11], for e.g. the third order susceptibility of baryon number ($\chi_B^{(3)}$) is related to the third moment ($< (\delta N_B)^3 >$) of baryon number distributions as $\chi_B^{(3)} =< (\delta N_B)^3 > /VT^3$; and $V, T$ are volume and temperature of system respectively. As volume of the system is hard to determine, the susceptibility ratio, such as $\chi_B^{(4)}/\chi_B^{(2)}$ and $\chi_B^{(3)}/\chi_B^{(2)}$, are used to compare with the experimental results. It has been found that the baryon number susceptibility ratio can be directly connected to the moment products of net-baryon number distributions as $\kappa\sigma^2 = \chi_B^{(4)}/\chi_B^{(2)}$ and $S\sigma = \chi_B^{(3)}/\chi_B^{(2)}$ [12]. Theoretical calculations also demonstrate that the experimental measurable net-proton number $N_{p-\bar{p}} = N_p - N_{\bar{p}}$ (number of protons minus number of anti-protons) event-by-event fluctuations can reflect the baryon, charge and strangeness number fluctuations and also sensitive to the correlation length [13]. Thus, we can use the higher order moments of the net-proton multiplicity distributions to search for the QCD critical point [14].

The paper is organized as follows. In section II we briefly discuss the UrQMD model used for the analysis presented here. In section III we define the observables.

*Electronic address: luoxf@phy.ccnu.edu.cn

Sections IV, V and VI discuss the measurement artifacts, centrality bin width effect (CBWE), centrality resolution effect (CRE) and Auto-correlations effect (ACE), respectively. In section VII we present different methods of estimating the statistical errors for moment analysis. Finally in section VIII we present a summary of the work.

## II. URQMD MODEL

The Ultra Relativistic Quantum Molecular Dynamics (UrQMD) is a microscopic many-body approach to $p+p$, $p+A$, and $A+A$ interactions at relativistic energies and is based on the covariant propagation of color strings, constituent quarks, and diquarks accompanied by mesonic and baryonic degrees of freedom. Furthermore it includes rescattering of particles, the excitation and fragmentation of color strings, and the formation and decay of hadronic resonances. UrQMD is a transport model for simulating heavy-ion collisions in the energy range from SIS to RHIC (even in LHC). It combines different reaction mechanism, and can provide theory simulation results of various experimental observables. The main parts of UrQMD model are: two body reaction cross section, two body potential and decay width. More details about the UrQMD model can be found in the reference [15].

We performed our calculations with UrQMD model for Au+Au collisions at $\sqrt{s_{NN}}$= 7.7, 11.5, 19.6, 27, 39, 62.4, 200 GeV and the corresponding event statistics are 107, 108, 50, 65, 93, 29 and 28 million, respectively. We measure event-by-event wise $N_{p-\bar{p}}$ at the mid-rapidity ($|y| < 0.5$) and within the transverse momentum $0.4 < p_T < 0.8$ GeV/c. This is same kinematic range used in moment analysis of net-proton distributions as in the STAR experiment [14, 16–18].

## III. OBSERVABLES

In statistics, probability density distribution functions can be characterized by the various moments, such as mean ($M$), variance ($\sigma^2$), skewness ($S$) and kurtosis ($\kappa$). Before introducing the above moments used in our analysis, we would like to define cumulants, which are alternative methods to the moments of a distribution. The cumulants determine the moments in the sense that any two probability distributions whose cumulants are identical will have identical moments as well, and similarly the moments determine the cumulants.

In the following, we use $N$ to represent the net-proton number $N_{p-\bar{p}}$ in one event. The average value over whole event ensemble is denoted by $< N >$, where the single angle brackets are used to indicate ensemble average of a event-by-event distribution.

The deviation of $N$ from its mean value is defined by

$$\delta N = N - < N > \tag{1}$$

The various order cumulants of event-by-event distributions of a variable $N$ are defined as:

$$C_{1,N} = < N > \tag{2}$$
$$C_{2,N} = < (\delta N)^2 > \tag{3}$$
$$C_{3,N} = < (\delta N)^3 > \tag{4}$$
$$C_{4,N} = < (\delta N)^4 > -3 < (\delta N)^2 >^2 \tag{5}$$

An important property of the cumulants is their additivity for independent variables. If $X$ and $Y$ are two independent random variables, then we have $C_{i,X+Y} = C_{i,X} + C_{i,Y}$ for $i$th order cumulant. This property will be used in our study.

Once we have the definition of cumulants, various moments can be obtained as:

$$M = C_{1,N}, \sigma^2 = C_{2,N}, S = \frac{C_{3,N}}{(C_{2,N})^{3/2}}, \kappa = \frac{C_{4,N}}{(C_{2,N})^2} \tag{6}$$

And also, the moments product $\kappa\sigma^2$ and $S\sigma$ can be expressed in terms of the ratio of cumulants like:

$$\kappa\sigma^2 = \frac{C_{4,N}}{C_{2,N}}, S\sigma = \frac{C_{3,N}}{C_{2,N}} \tag{7}$$

With above definition of various moments, we can calculate various moments and moment products from the measured event-by-event net-proton distribution for each centrality.

## IV. CENTRALITY BIN WIDTH EFFECT (CBWE) AND CORRECTION

To avoid the ACE and CRE (will be discuss later), the centralities in the UrQMD calculations are defined by the charged kaon and pion multiplicity within $|\eta| < 2$. Experimentally, the centrality is usually expressed as a percentage of the total cross-section, such as $0-5\%$ (most central), $30-50\%$ (semi- peripheral), which indicates the fraction of a data sample(corrected for efficiency) relative to all possible collision geometries (impact parameters). Before calculating various moments of net-proton distributions for one wide centrality bin, such as $0-5\%$, $5-10\%$ , we should consider the so called Centrality Bin Width Effect (CBWE) arising from the impact parameter (or volume) variations due to the finite centrality bin. This effect must be eliminated or at least reduced, as an artificial centrality dependence could be introduced due to finite centrality bin width.

To formulate and demonstrate the centrality bin width effect, we write the event-by-event net-proton distributions in one centrality as

$$P(N) = \sum_i \omega_i f^{(i)}(N), (\sum_i \omega_i = 1) \tag{8}$$

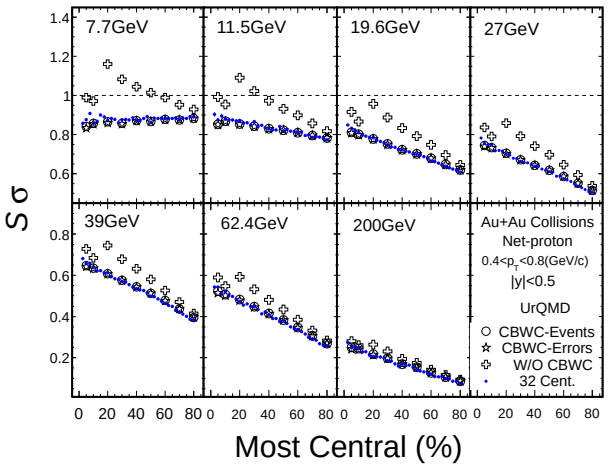


FIG. 1: (Color online) The centrality dependence of the moments products ($S\sigma$) of net-proton multiplicity distributions for Au+Au collisions at $\sqrt{s_{NN}}$=7.7, 11.5, 19.6, 27, 39, 62.4, 200GeV in UrQMD model. The dots represent the result of 32 centralities.

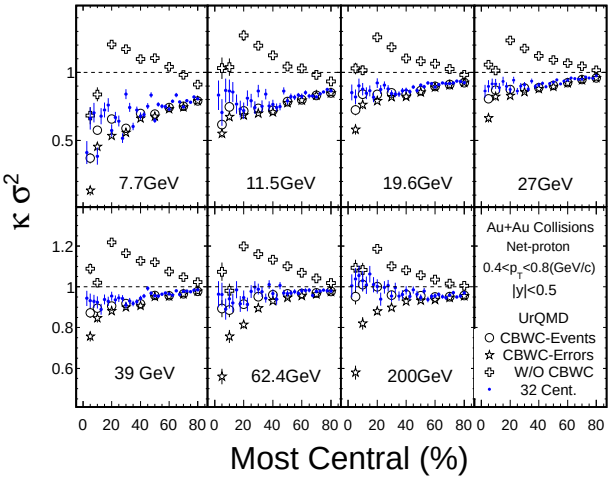


FIG. 2: (Color online) The centrality dependence of the moments products ($\kappa\sigma^2$) of net-proton multiplicity distributions for Au+Au collisions at $\sqrt{s_{NN}}$=7.7, 11.5, 19.6, 27, 39, 62.4, 200GeV in UrQMD model. The dots represent the result of 32 centralities.

, where the $\omega_i$ and $f^{(i)}(N)$ are the weighted and net-proton distributions for $i_{th}$ impact parameter in one centrality, respectively. From eqs. (2)-(5) and (8), we can calculate the various order cumulants for the distribution $P(N)$ as below:

$$C_{1,N} = \sum_i \omega_i C^i_{1,N} = \sum_i \omega_i < N >_i \quad (9)$$

$$C_{2,N} = (\sum_i \omega_i C^i_{2,N}) + C'_{2,C^i_{1,N}} \quad (10)$$

$$C_{3,N} = (\sum_i \omega_i C^i_{3,N}) + C'_{3,C^i_{1,N}} + 3 \times C'_{1,C^i_{1,N},1,C^i_{2,N}} \quad (11)$$

$$\begin{aligned} C_{4,N} &= (\sum_i \omega_i C^i_{4,N}) + C'_{4,C^i_{1,N}} + 4 \times C'_{1,C^i_{1,N},1,C^i_{3,N}} \\ &+ 6 \times C'_{1,(C^i_{1,N})^2,1,C^i_{2,N}} - 12 \times (C'_{1,C^i_{1,N}})(C'_{1,C^i_{1,N},1,C^i_{2,N}}) \\ &- 3 \times (C'_{2,C^i_{1,N}})^2 + 3 \times C'_{2,C^i_{2,N}} \end{aligned} \quad (12)$$

, where the $C^i_{k,N}$ $(k = 1,2,3,4)$ are the $k^{th}$ order cumulant for net-proton distribution $f^{(i)}(N)$; the $C'_{k,X}$ $(X = C^i_{m,N},\ k,m = 1,2,3,4)$ are $k^{th}$ order cutmulant for random variable $X = C^i_{m,N}$ under the discrete probability distribution $Prob(X)$=$\omega_i$; the $C'_{1,X,1,Y}$=$< XY > - < X >< Y >$ $(X = C^i_{k,N},\ k = 1,2,3,4)$ are the first order joint cumulant for random variable $X, Y$ under the discrete probability distribution $Prob(X,Y)$=$\omega_i$. We may find that the higher order cumulants $C_{k,N}$ $(k = 1,2,3,4)$ can be expressed by the addition of two parts, one is the weighted average of the same order cumulant of each sub-distribution $f^{(i)}(N)$, and the other part is the cumulant of lower order under the discrete weighted distributions, which stems from the fluctuation of impact parameters within the centrality and results in the centrality bin width effect.

Experimentally, the centrality is usually determined by an observable like the charged particle multiplicity and the smallest centrality bin is determined by a single multiplicity value. Generally, experiments report the results for a wider centrality bin, such as $0-5\%$,$5-10\%$,...etc., to supress the statistical fluctuations. To eliminate the centrality bin width effect, we have developed a technique, called Centrality Bin Width Correction (CBWC), to calculate the various moment for each multiplicity in one wide centrality bin. The method has the weighted averaged by the number of events in each multiplicity.

$$\sigma = \frac{\sum_r n_r \sigma_r}{\sum_r n_r} = \sum_r \omega_r \sigma_r \quad (13)$$

$$S = \frac{\sum_r n_r S_r}{\sum_r n_r} = \sum_r \omega_r S_r \quad (14)$$

$$\kappa = \frac{\sum_r n_r \kappa_r}{\sum_r n_r} = \sum_r \omega_r \kappa_r \quad (15)$$

, where the $n_r$ is the number of events in $r^{th}$ multiplicity and the corresponding weight $\omega_r = n_r / \sum_r n_r$.

Fig. 1 and Fig. 2 show the centrality dependence of the moment products $(S\sigma, \kappa\sigma^2)$ of net-proton multiplicity distributions for Au+Au collisions $\sqrt{s_{NN}}$=7.7, 11.5, 19.6, 27, 39, 62.4 and 200 GeV in the UrQMD model. The open circle and open cross in Fig. 1 and 2 represent the results calculated with and without technique of CBWC in the nine centralities (0-5%, 5-10%, 10-20%, 20-30% ...), respectively. The solid circles show the result of centrality dependence of 32 bins in centrality (0-2.5%, 2.5-5%, 5-7.5%...), in which the CBWC is not applied. We can see clearly that the results with CBWC are very different from the results without CBWC. It means the CBWE do have a significant contribution to the value of the moment analysis and the CBWC will make the value of the moment products smaller by reducing the effect of variation of volume in one wide centrality bin. On the other hand, the results of 32 centralities, for which the CBWE is small, are good agreement with the result from nine centralities with CBWC, which indicates the effectiveness of the proposed CBWC method. So, before we perform higher order moments calculation in one wide centrality in heavy-ion collisions, the CBWC should be applied to reduce the effect of variation of the volume within the centrality bin width.

We also try to use error weighted method to do the CBWC (open star in Fig. 1 and 2) by replacing the weight factor $n_r$ in Equ. (13)-(15) with $1/error^2$ for each single multiplicity. The error is obtained with Delta theorem, which will be discussed later. We find that the results with error weighted CBWC are consistent with the results with events weighted CBWC and the results with 32 centralities for $S\sigma$, but not for $\kappa\sigma^2$. It means the error weighted method can not be used for CBWC, which may be due to the error being not only related to the number of events but also the moments itself.

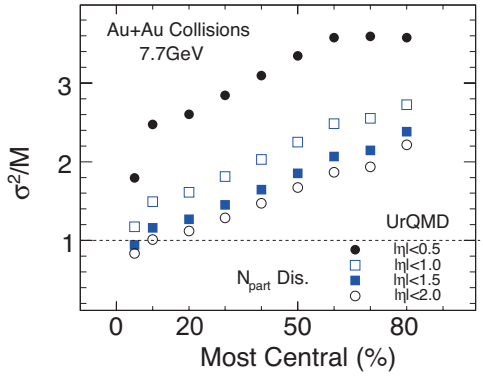


FIG. 3: (Color online) The centrality dependence of the $\sigma^2/M$ of net-proton multiplicity distributions for Au+Au collisions at $\sqrt{s_{NN}}$=7.7, 11.5, 19.6, 27, 39, 62.4, 200GeV in UrQMD model.

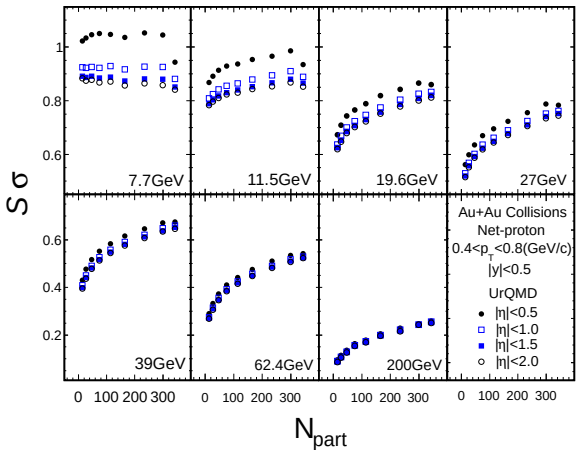


FIG. 4: (Color online) The centrality dependence of the moments products $S\sigma$ of net-proton multiplicity distributions for Au+Au collisions at $\sqrt{s_{NN}}$=7.7, 11.5, 19.6, 27, 39, 62.4, 200GeV in UrQMD model.

## V. CENTRALITY RESOLUTION EFFECT

The definition of the centralities in heavy-ion collisions is not unique and can be defined through different quantities. A frequently used quantity is the so called impact parameter b, defined as the distance between the geometrical centers of the colliding nuclei in the plane transverse to their direction. Other variables, such as the number of participant nucleons, $N_{part}$ and the number of binary collisions, $N_{coll}$, can be also used. Unfortunately, those geometry variables can't be directly measured in the heavy-ion collision experiment and the collision centrality is determined from a comparison between experimental measures such as the particle multiplicity and Glauber Monte-Carlo simulations [19]. Particle multiplicity, not only depends on the physics processes, but also reflects the initial geometry of the heavy-ion collision. This indicates that relation between measured particle multiplicity and impact parameter is not one-to-one correspond and there are fluctuations in the particle multiplicity even for a fixed impact parameter. Thus, it could have different initial collision geometry resolution (centrality resolution) for different centrality definitions with particle multiplicity. Fig. 3 shows the centrality dependence of $\sigma^2/M$ of number of participant nucleons ($N_{part}$) distributions for Au+Au collisions at $\sqrt{s_{NN}}$=7.7 GeV in UrQMD model. As the $N_{part}$ can reflect the initial geometry (volume) of the colliding nuclei, the $\sigma^2/M$ of $N_{part}$ multiplicity distributions can be regarded as the centrality resolution for a certain centrality definition. It means if less particles are used to define the collision centrality,

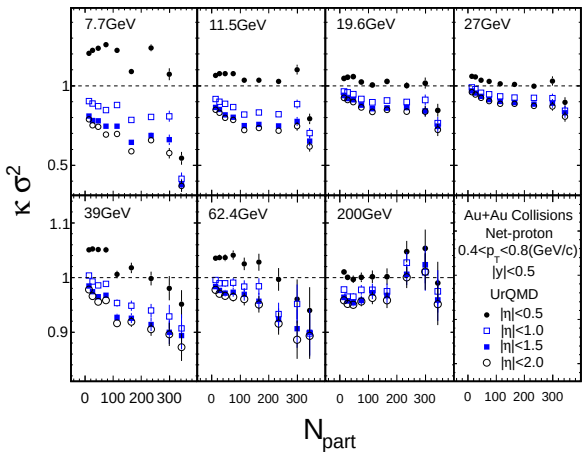


FIG. 5: (Color online) The centrality dependence of the moments products $\kappa\sigma^2$ of net-proton multiplicity distributions for Au+Au collisions at $\sqrt{s_{NN}}$=7.7, 11.5, 19.6, 27, 39, 62.4, 200GeV in UrQMD model.

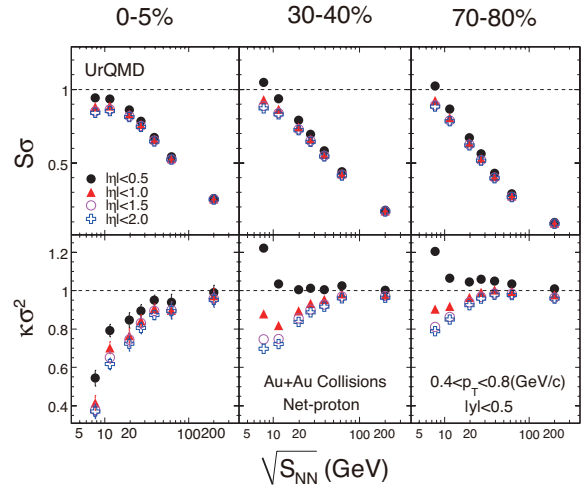


FIG. 6: (Color online) The energy dependence of the moments products $(S\sigma, \kappa\sigma^2)$ of net-proton multiplicity distributions for Au+Au collisions at $\sqrt{s_{NN}}$=7.7, 11.5, 19.6, 27, 39, 62.4, 200GeV in UrQMD model.

then larger initial geometry (volume) fluctuations will be observed. This may affect the moment analysis of particle multiplicity distributions. To verify this effect in the moment analysis, we use the charged kaon and pion multiplicity produced in the final state within $|\eta| < 0.5, 1, 1.5$ and 2 to define the centrality in the UrQMD calculations. Fig. 4 and 5 shows the centrality dependence of the moment products $(S\sigma, \kappa\sigma^2)$ of net-proton multiplicity distributions for four different $\eta$ range of charged kaon and pion used to determine the centrality. When we increase the $\eta$ range ($|\eta| < 1, 1.5, 2$), the values of $S\sigma$ and $\kappa\sigma^2$ will decreases. We observe significant difference for moment products $(S\sigma, \kappa\sigma^2)$ for the different $\eta$ range of the centrality definition. The behavior can be understood as due to reduced contribution from volume fluctuations arising from centrality definition. On the other hand, the moment products $(S\sigma, \kappa\sigma^2)$ show saturation at $|\eta| < 2$. The centrality resolution effect by now gets largely suppressed. Fig. 6 shows the energy dependence of moment product $(S\sigma, \kappa\sigma^2)$ of net-proton multiplicity distributions for three different centralities $(0-5\%, 30-40\%, 70-80\%)$ with four different $\eta$ coverage in Au+Au collisions. We can find that the fourth order fluctuation is more sensitive to the centrality resolution effect than the third order fluctuation, and it has larger effect in the peripheral collision as well as at low energies. Thus, we should use a lager $\eta$ coverage in the centrality definition for the real experimental moment analysis to reduce the centrality resolution effects.

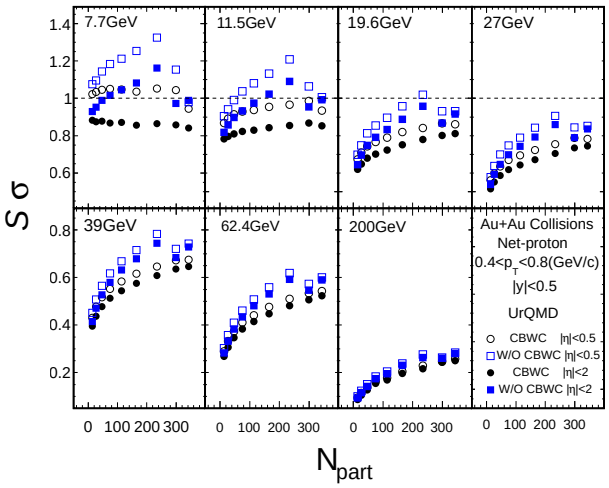


FIG. 7: (Color online) The centrality dependence of the moments products $S\sigma$ of net-proton multiplicity distributions for Au+Au collisions at $\sqrt{s_{NN}}$=7.7, 11.5, 19.6, 27, 39, 62.4, 200GeV in UrQMD model. The open square and circle are the results with CBWC and without CBWC at $|\eta| < 0.5$ for centrality definition. The solid square and circle are the results with CBWC and without CBWC at $|\eta| < 2$ for centrality definition.

Fig. 7 and 8 show the centrality dependence of moment products $(S\sigma, \kappa\sigma^2)$ of net-proton multiplicity distributions for Au+Au collisions with CBWC and without CBWC at different centrality resolution ($|\eta| < 0.5, 2$). We can see that the CBWE and CRE have larger effect in the moment products at low energies than at high energies. The magnitude of CBWE in the moment products is comparable with the magnitude of CRE at low energies, while the CBWE has larger effects at higher energies.

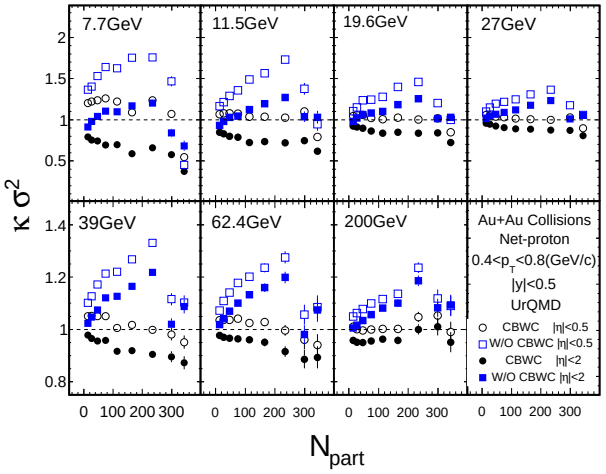


FIG. 8: (Color online) The centrality dependence of the moment products $\kappa\sigma^2$ of net-proton multiplicity distributions for Au+Au collisions at $\sqrt{s_{NN}}$=7.7, 11.5, 19.6, 27, 39, 62.4, 200GeV in UrQMD model. The open square and circle are the results with CBWC and without CBWC at $|\eta| < 0.5$ for centrality definition. The solid square and circle are the results with CBWC and without CBWC at $|\eta| < 2$ for centrality definition.

Let's summarize the CBWE and the CRE in the moment analysis in heavy-ion collisions. The CBWE stems from the variation of the volume when we perform the moment calculations within one wide centrality bin and the CRE is originated from the initial geometry (volume) fluctuations of the colliding nuclei. Both of these two effects are resulted from the volume effects and it can be effectively suppressed by using the CBWC and more particles (larger $\eta$ coverage) in centrality definition, respectively.

## VI. AUTO-CORRELATION EFFECT

In the above sections, we use the multiplicity of charged kaon and pion to define the centrality, not all of the charged particles. The reason is to avoid the effect of auto-correlation between protons/anti-protons involved in our moments analysis and in the centrality definition. If the charged particles for the centrality definition contains the proton and anti-proton used in our moments analysis, it will introduce auto-correlation effect. Fig. 9 shows the proton distribution in the phase space of transverse momentum ($p_T$) and rapidity ($y$) for Au+Au collisions at $\sqrt{s_{NN}}$=19.6 GeV in the UrQMD model. The protons used in the moment analysis are distributed in the oblong box ($0.4 < p_T < 0.8$ GeV/c, $|y| < 0.5$). The solid curve represents ($p_T$, $y$) points with $\eta = 2$. If all the charged particles within the $\eta = 2$ curve are used to define the centrality, it will definitely introduce the auto-correlation effects.

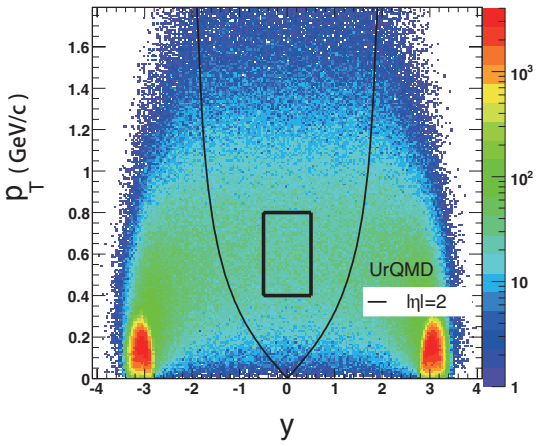


FIG. 9: (Color online) The proton distribution in the phase space of transverse momentum ($p_T$ GeV/c) and rapidity ($y$) for Au+Au collisions at $\sqrt{s_{NN}}$=19.6 GeV using the UrQMD model. The relation between $p_T$ and $y$ is $p_T = m_0/\sqrt{\sinh^2\eta/\sinh^2 y - 1}$, where the $m_0$ is the particle rest mass.

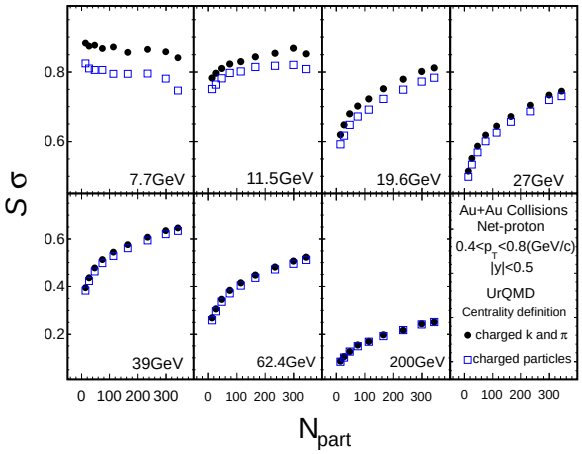


FIG. 10: (Color online) The centrality dependence of the moments products $S\sigma$ of net-proton multiplicity distributions for Au+Au collisions at $\sqrt{s_{NN}}$=7.7, 11.5, 19.6, 27, 39, 62.4, 200GeV in UrQMD model.

Fig. 10 and 11 show the centrality dependence of the moment products $S\sigma$ and $\kappa\sigma^2$ of net-proton distributions at centrality definition with charged particles (open squares) and charged kaon and pion (solid circles). An obvious difference between the results from the two types of centrality definition can be observed. This is because that if the protons and anti-protons used in the moments

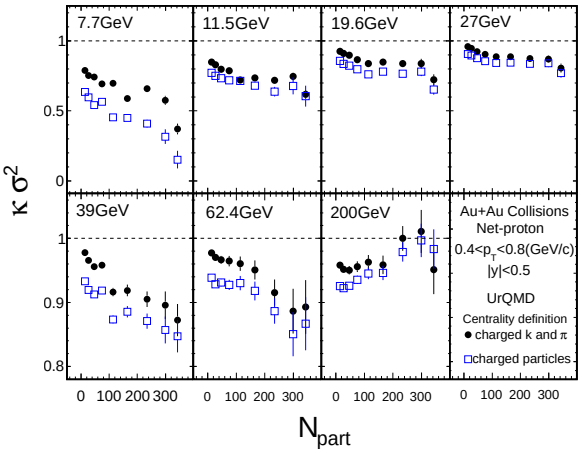


FIG. 11: (Color online) The centrality dependence of the moments products $\kappa\sigma^2$ of net-proton multiplicity distributions for Au+Au collisions at $\sqrt{s_{NN}}$=7.7, 11.5, 19.6, 27, 39, 62.4, 200GeV in UrQMD model.

analysis are also used in the centrality definition, it introduces an auto-correlation effect in the final results. So, to avoid the auto-correlation effect, we should exclude the corresponding proton/anti-protons from the centrality definition.

## VII. STATISTICAL ERROR ESTIMATION

As the moment analysis is a statistics hungry study, the error estimation is crucial to extract physics information from the limited experimental data. We will present several statistics methods (Delta theorem, Bootstrap [20], Sub-group) of error estimation in the moment analysis and discuss their comparisons through a Monte Carlo simulation. For simplicity, we assume the particles are independently distributed as Poissonian distributions. Then, the difference of two independent Poisson distributions is distributed as "Skellam" distribution. The skellam probability density distribution is

$$f(k;\mu_1,\mu_2) = e^{\mu_1+\mu_2}(\frac{\mu_1}{\mu_2})^{k/2} I_{|k|}(2\sqrt{\mu_1\mu_2}) \quad (16)$$

, where the $\mu_1$ and $\mu_2$ are the mean value of the Poisson distributions, respectively, the $I_k(z)$ is the modified bessel function of the first kind. Then, we can calculate various moments $(M,\sigma,S,\kappa)$ and moment products $(\kappa\sigma^2, S\sigma)$ products of the Skellam distribution. The relations are given below:

$$M = \mu_1 - \mu_2, \sigma = \sqrt{\mu_1+\mu_2} \quad (17)$$

$$S = \frac{\mu_1-\mu_2}{(\mu_1+\mu_2)^{2/3}}, \kappa = \frac{1}{\mu_1+\mu_2} \quad (18)$$

$$S\sigma = \frac{\mu_1-\mu_2}{\mu_1+\mu_2}, \kappa\sigma^2 = 1 \quad (19)$$

To do the simulation, we set the two mean values of the Skellam distributions as $\mu_1 = 4.11$, $\mu_2 = 2.99$, which are similar with the mean proton and anti-proton numbers measured in central Au+Au collisions at $\sqrt{s_{NN}}$= 200 GeV by the STAR experiment [16]. Then, we generate random numbers as per the Skellam distribution. The details of Delta theorem error estimation method for moment analysis can be found in [21]. The bootstrap method [20] is based on the repeat sampling with the same statistics of the parent distribution and the statistical errors can be obtained as the root mean square of the observable from each sample. In Sub-group method, we randomly divide the whole sample into several subgroups with same statistics and the errors are obtained as the root mean square of the observable from each subgroup. In our simulation, we set 200 bootstrap times and 5 sub-groups.

Fig. 12 shows the error estimation comparison between Delta theorem, Bootstrap and Sub-group methods for $\kappa\sigma^2$ of Skellam distribution. For each method, fifty independent samples are sampled from the Skellam distribution with statistics 0.01 , 0.1 and 1 million, respectively. The probability for the value staying within $\pm1\sigma$ around expectation is about 68.3% and it means error bars of 33 out of 50 points should touch the expected value(dashed line at unity) in Fig. 12. We find that the results from the Delta theorem and Bootstrap method show similar error values and satisfies the above criteria, while the random sub-group method over estimates the statistical errors. It indicates that the Delta theorem and Bootstrap error estimation methods for the moment analysis are reasonable and can reflect the statistical properties of moments.

According to the error formula derived from delta theorem, for normal distributions, the errors for cumulants ratios are proportional to the standard deviation of the distribution as:

$$error(\hat{S}\hat{\sigma}) \propto \frac{\sigma}{\sqrt{n}} \quad (20)$$

$$error(\hat{\kappa}\hat{\sigma}^2) \propto \frac{\sigma^2}{\sqrt{n}} \quad (21)$$

, where the $n$ is the number of events.

## VIII. SUMMARY

We presented three measurement artifacts in the moments analysis of net-proton distributions in heavy-ion collisions using the UrQMD model. These are centrality

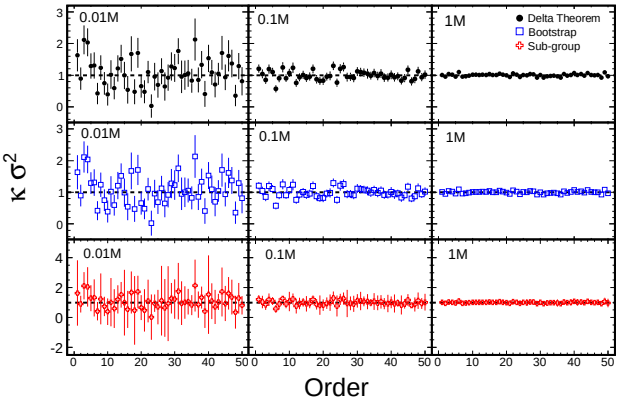


FIG. 12: (Color online) $\kappa\sigma^2$ for 50 samples that independently and randomly generated from the Skellam distribution with different number of events (0.01, 0.1, 1 million). The dashed lines are expectations value 1.

bin width effect, centrality resolution effect and auto-correlation effect. The UrQMD calculations are carried out for Au+Au collisions at $\sqrt{s_{NN}}$= 7.7, 11.5, 19.6, 27, 39, 62.4, 200 GeV. We also discussed corresponding techniques to suppress those effects to obtain physics information. The centrality bin width effect and centrality resolution effect are originated from the volume and its fluctuations. The auto-correlation effect is resulted from using the same particles for the moment analysis and for the centrality definitions. We have also discussed the error estimation method used in moments analysis. The effects and techniques discussed in this paper are not only restricted within the net-proton analysis, but also applicable to other particle species, such as net-charge, net-strangeness.

## Acknowledgments

The work was supported in part by the National Natural Science Foundation of China under grant No. 11205067 and 11135011. CCNU-QLPL Innovation Fund(QLPL2011P01) and China Postdoctoral Science Foundation (2012M511237). BM is supported by the DST SwarnaJayanti project fellowship.

## References

[1] R. V. Gavai, S. Gupta, Phys. Rev. D **78**, 114503 (2008).
[2] M. M. Aggarwal *et al.* (STAR Collaboration), arXiv: 1007.2613.
[3] Y. Aoki *et al.*, Nature **443** 675 (2006).
[4] S. Ejiri, Phys. Rev. D **78** (2008) 074507 ; E. S. Bowman, J. I. Kapusta, Phys. Rev. C **79** (2009) 015202.
[5] Y. Aoki *et al.*, Phys. Lett. B **643** (2006) 46; M. Cheng *et al.*, Phys. Rev. D **74**, 054507 (2006).
[6] M. A. Stephanov, Int. J. Mod. Phys. A **20**, 4387 (2005); B. Mohanty, Nucl. Phys. A **830**, 899c (2009).
[7] Z. Fodor, S. D. Katz, Phys. Lett. B **534** (2002) 87; Philippe de Forcrand and O. Philipsen, Nucl. Phys. B **642** (2002) 290; R. V. Gavai, S. Gupta, Phys. Rev. D **68** (2003) 034506.
[8] M. A. Stephanov, Phys. Rev. Lett. **102**, 032301 (2009).
[9] M. Cheng *et al.*, Phys. Rev. D **79**, 074505 (2009). A. Bazavov, *et al.*, arXiv:1203.0784.
[10] S. Borsanyi *et al.*, JHEP **1201**, 138 (2011).
[11] F. Karsch and K. Redlich, Phys. Lett. B **695**, 136 (2011).
[12] S. Gupta, X. Luo, B. Mohanty, H. G. Ritter, N. Xu, Science **332**, 1525 (2011).
[13] Y. Hatta and M. A. Stephanov, Phys. Rev. Lett. **91**, 102003 (2003).
[14] X. Luo (for the STAR Collaboration), arXiv:1210.5573.
[15] M. Bleicher *et al.*, J. Phys. G: Nucl. Part. Phys. **25**, 1859 (1999).
[16] M. M. Aggarwal *et al.* (STAR Collaboration), Phys. Rev. Lett. **105**, 022302 (2010).
[17] X. Luo (for the STAR Collaboration), J. Phys.: Conf. Ser. **316**, 012003 (2011).
[18] X. Luo (for the STAR Collaboration), Acta Phys. Pol. B Proc. Supp.**5**, 497 (2012). [arXiv:1111.5671].
[19] Michael L. Miller*et al.*, Ann. Rev. Nucl. Part. Sci. **57**, 205 (2007).
[20] B. Efron,R. Tibshirani, An introduction to the bootstrap, Chapman & Hall (1993).
[21] X. Luo, J. Phys. G: Nucl. Part. Phys. **39**, 025008 (2012).